Analytica Chimica Acta 1155 (2021) 338357

Contents lists available at ScienceDirect

Analytica Chimica Acta

journal homepage: www.elsevier.com/locate/aca

A colorimetric sensor for acid phosphatase activity detection based on acridone derivative as visible-light-stimulated oxidase mimic

Tao Zhang [a, 1], Wenhui He [a, b, 1], Xiaodan Song [b, c], Dongzhi Wu [a], Yaokun Xia [b, c], Yan Liu [a], Linzhao Wu [a], Weiming Sun [c, d, ***], Fengfei Lin [a, e, **], Jinghua Chen [b, c, *]

[a] Department of Orthopedics Institute, Fuzhou Second Hospital Affiliated to Xiamen University, Fuzhou, 350007, PR China
[b] Department of Pharmaceutical Analysis, The School of Pharmacy, Fujian Medical University, Fuzhou, Fujian Province, 350122, PR China
[c] Fujian Key Laboratory of Drug Target Discovery and Structural and Functional Research, The School of Pharmacy, Fujian Medical University, Fuzhou, Fujian Province, 350122, PR China
[d] Department of Basic Chemistry, The School of Pharmacy, Fujian Medical University, Fuzhou, Fujian Province, 350122, PR China
[e] Department of Orthopaedic Trauma, Fuzhou Second Hospital Affiliated to Xiamen University, Fuzhou, 350007, PR China

HIGHLIGHTS

- An acridone derivative 10-benzyl-2-amino-acridone (BAA) is synthesized.
- The BAA exhibits an intrinsic visible-light-stimulated oxidase-like activity.
- The BAA shows higher catalytic efficiency for TMB than our previous work.
- A selective colorimetric sensing strategy is designed to detect ACP.

GRAPHICAL ABSTRACT

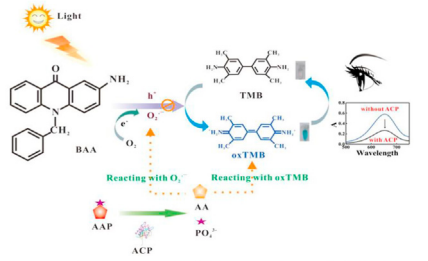

Schematic illustration of the colorimetric sensing strategy for ACP detection

ARTICLE INFO

Article history:
Received 23 November 2020
Received in revised form
21 February 2021
Accepted 26 February 2021
Available online 27 February 2021

Keywords:
10-Benzyl-2-amino-acridone
Visible-light-stimulated oxidase-like activity
ACP activity detection

ABSTRACT

Currently, organic artificial enzymes as biocatalysts have been extensively used to construct various colorimetric sensors. However, exploiting a potential organic artificial enzyme with high catalytic efficiency still remains a challenge. To address this issue, herein, we synthesize an acridone derivative 10-benzyl-2-amino-acridone (BAA). The synthesized BAA exhibits an intrinsic visible-light-stimulated oxidase-like activity, which is capable of oxidizing various chromogenic substrates without destructive hydrogen peroxide (H_2O_2) under visible light stimulation, resulting in colored products. The reaction system can be regulated by switching light on and off, which is milder and more reliable means than others H_2O_2-dependent. The photocatalytic mechanism of BAA is investigated in detail. However, L-ascorbic acid (AA), an antioxidant generating from the acid phosphatase (ACP)-mediated hydrolysis of 2-phospho-L-ascorbic acid (AAP), is able to inhibit the catalytic activity of BAA. Based on the above properties, a facile, photo-switchable and low-cost colorimetric sensing strategy is developed for ACP

* Corresponding author. , Department of Pharmaceutical Analysis, The School of Pharmacy, Fujian Medical University, Fuzhou, Fujian Province, 350122, PR China.
** Corresponding author. , Department of Orthopedics Institute, Fuzhou Second Hospital Affiliated to Xiamen University, Fuzhou, 350007, PR China.
*** Corresponding author. , Fujian Key Laboratory of Drug Target Discovery and Structural and Functional Research, The School of Pharmacy, Fujian Medical University, Fuzhou, Fujian Province, 350122, PR China.
E-mail addresses: sunwm@fjmu.edu.cn (W. Sun), 596558644@qq.com (F. Lin), cjh_huaxue@126.com (J. Chen).
[1] Tao Zhang and Wenhui He make equal contribution to the paper.

https://doi.org/10.1016/j.aca.2021.338357

detection. The linear range is 0.05−2.5 U/L (r = 0.9994), and the limit of detection (LOD) is 0.0415 U/L. Moreover, the proposed sensing system can be applied for monitoring ACP activity in practical samples, demonstrating promising applications in clinical analysis and biosensor platform.

1. Introduction

Colorimetric sensor was a promising tool in cancer diagnosis field given its brilliant merits such as simplicity, intuition and convenience [1]. Especially, enzymatic reaction opened up new possibilities for the construction of colorimetric sensors, which has been widely applied for the detection of tumor markers such as small molecule, DNA and protein [2−4]. However, most of these enzymes were natural enzymes, which still suffered some intrinsic limitations containing high cost, poor stability and easily denatured [5,6]. Substantial researchers, therefore, were devoted to exploit promising alternatives such as nanozymes [7−9], metal-organic frameworks [10], and small molecule mimic enzymes [11]. Although great achievements have been made, they still have many shortcomings. For example, some enzymes were dependent on H_2O_2 for high catalytic activity. As we all known, H_2O_2, a strong oxidant, was unstable and destructive, which not only could be easily decomposed and lost its oxidative capacity, but also caused the inactivation of biological macromolecules in the sensing system [12,13]. And some were difficult to efficiently modulate their catalytic activities [14]. To overcome these shortcomings, a new tunable and mild means for inducing catalytic activity is appealing.

Compared with these enzymes, as described above, the photo-induced oxidase mimic was a viable candidate for the development of biosensors, which showed numerous merits [15,16]. For example, the catalytic system could be adjustable by controlling light irradiation intensity and time, which was a simple, rapid, green and safe means for obtaining the catalytic activity. On the other hand, the reaction process avoided the use of unstable and destructive H_2O_2, which was more suitable for biosensing systems. Up to now, a large variety of nanomaterials such as gold nanoparticles [17], CdS quantum dots [18], TiO_2 [13], and AgX nanoparticles [19] have been found possessing photo-induced oxidase-like activity that can catalyze the oxidation substrate without H_2O_2 by visible light triggering. However, these inorganic nanozymes were restricted by weak visible absorption [14,15] and uncertain toxicity [20]. At present, the organic small molecules have emerged as ideal candidates for photoresponsive oxidase mimics due to their strong visible light absorption [14]. For example, Liu et al. proposed a visual sensing strategy based on photocatalytic activity of fluorescein for detection of carboxylesterase [21]. Zhang et al. discovered dsDNA-SYBR Green I complex holding photocatalytic activity and used it for label-free and universal colorimetric bioassay [22]. Therefore, the design and synthesis of organic small molecules with photoinduced mimic enzyme activity have became a research hotspot in recent years.

Acridone derivatives, as a class of nitrogen-containing heterocyclic organic small molecules, have been attracted tremendous attentions due to their series of features such as simple structure, flexible modification, conjugated planes, and tunable electron donor-acceptor system [23,24]. With the development of research, increasingly properties of acridone derivatives, such as favorable pharmacological activities [25], fast electrochemical response [26], and high fluorescence signal [27], have been uncovered for the construction of various biosensors. However, there are few reports concerning the enzyme-mimicking property of acridone derivatives. Recently, our group was also devoted to the study of acridone derivatives and found that 10-methyl-2-amino-acridone (MAA) possessed visible-light-induced oxidase-like activity, but its catalytic activity for TMB was low owing to the substituents [28,29]. To improve catalytic efficiency of acridone derivative, we synthesized 10-benzyl-2-amino-acridone (BAA). The synthesized BAA showed an intrinsic visible-light-stimulated oxidase-like activity, which could catalyze various substrates including 3,3′,5,5′-tetramethylbenzidine (TMB), ophenylenediamine (OPD) and 2,2′-azinobis (3-ethylbenzthiazoline-6-sulfonic acid) diammonium salt (ABTS), and its catalytic efficiency for TMB was higher than our previous work. Hence, we constructed a photo-switchable, low-cost, selective and visual colorimetric sensing approach for monitoring ACP activity by using BAA as colorimetric probe. As shown in Scheme 1, under light irradiation, the BAA could produce $O_2^{\bullet-}$ and h^+ reactive species for oxidizing colorless TMB to blue products oxidized TMB (oxTMB). However, the catalytic activity of BAA could be suppressed by AA obtaining from the ACP-mediated hydrolysis of AAP, resulting in the generation of oxTMB decreased and accompanying with a visible color change, which was able to directly readout by the naked eye. That is, in presence of ACP, the ultraviolet absorption and color of reaction solution could be changed, thus realizing the ACP detection. This study provided a new ideal on the enzyme-mimicking property of acridone derivatives in future biosensors fields.

2. Experimental section

2.1. Chemicals and materials

Acridone (AR, 98%) was provided from Macklin Reagent Company. Benzyl bromide was purchased from West Asia Chemical Industry Co. Ltd. (Shandong, China). Proteinase K, lysozyme, urease, α-glucosidase, catalase (CAT), horseradish peroxidase were bought from Beijing Solarbio Sciences & Technology Co. Ltd. (Beijing, China). Sodium sulfide was purchased from Aladdin Reagent Co. Ltd. (Shanghai, China). TMB was derived from Tokyo Chemical Industry (TCI, Shanghai). AAP, ACP, pyrophosphatase, alkaline phosphatase, superoxide dismutase (SOD),N-ethylmaleimide (NEM), glutathione (GSH) and L-Cysteine were obtained from Sigma-Aldrich Chemical Co. Ltd. (Shanghai, China). N, N-dimethyl formamide (DMF), sodium acetate, acetate acid, nitric acid, absolute ethanol, EDTA, ammonium oxalate (AO), potassium iodide (KI), isopropanol (IPA), tert butanol (TBA), NaN_3, OPD, ABTS were obtained from Sinopharm Chemical Reagent Co. Ltd. (Shanghai, China). ACP assay kit was provided by Beyotime Biotechnology Co. Ltd. (Shanghai, China). The reagents used in all experiments were analytical grade and could be used directly without further treatment. All the water used in the experiment was ultra-pure water (18.2 MΩ, Milli-Q, Millipore).

2.2. Apparatus

The preparative high performance liquid chromatography (HPLC) (LC-20AP, Shimadzu, Japan) was used to separate and purify BAA. Photocurrent signals were recorded using an Electrochemical

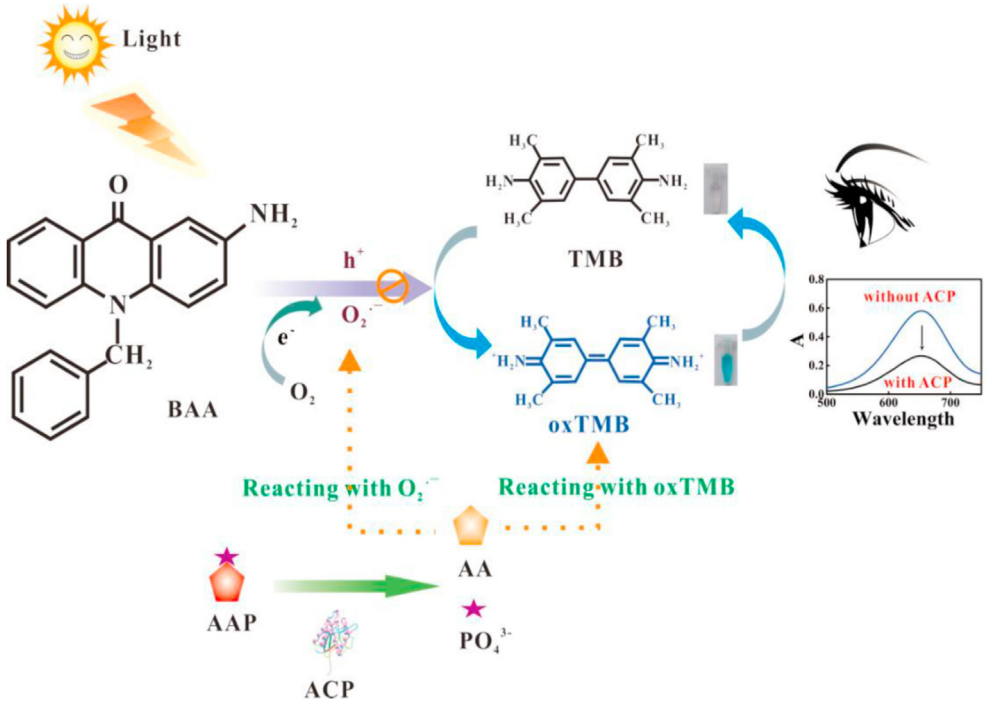

Scheme 1. Schematic illustration of the colorimetric sensing strategy for ACP detection.

analyzer (CHI 660E, Shanghai Chen Hua Instrument Co. Ltd. China). The visible light irradiation source was provided by a xenon lamp (300 W, Beijing NewBide Technology Co. Ltd. China) equipped with an ultraviolet cutoff filter ($\lambda \geq 400$ nm). The UV–vis absorption spectra were measured by Microplate Reader (Multiskan Go, Thermo Fisher Scientific, USA).

2.3. Synthesis of BAA

The BAA was synthesized referring to our previous works with an appropriate modification [24,28]. The detail experimental process was provided in Supporting Information.

2.4. Optical behavior of BAA

The sample solutions were transferred to quartz fluorescent cuvettes for detection by Cary Eclipse fluorescence spectrophotometer (Agilent, USA). The fluorescence measurement conditions were as follow: the excitation wavelength was 380 nm with an emission spectrum ranging from 400 nm to 690 nm, and the excitation and emission slits both were 5 nm. The UV–vis absorption spectrum was obtained by Cary 60 ultraviolet spectrophotometer (Agilent, USA) ranging from 230 to 500 nm.

2.5. Visible-light-stimulated oxidase-like activity of BAA

The visible-light-stimulated oxidase-like activity of BAA was studied by various substrates (TMB, OPD and ABTS). Typically, 400 μL of 10 mM acetate buffer solution (pH = 4.0), containing 10 μM BAA and 500 μM TMB (or 500 μM OPD or 1 mM ABTS), was reacted for 3 min under visible light. Then, the blue (or yellow or green) product was tested by Microplate Reader.

2.6. Colorimetric detection of ACP

Firstly, the mixture solution with 100 μL of AAP (4 mM) and 100 μL of various ACP concentrations was incubated at 37 °C for 30 min. Afterwards, 176 μL of 10 mM acetate buffer solution (pH = 4.0), 4 μL of 1 mM BAA and 20 μL of 10 mM TMB were introduced into the above solution and reacted for 3 min under visible light. Finally, the mixed solution was measured by Microplate Reader and the A_{652} value was gathered.

2.7. ACP inhibitor investigation

Firstly, 200 μL of 10 mM acetate buffer solution (pH = 4.0) containing 2 mM AAP, 5 U/L ACP, and different concentrations of NaF was incubated at 37 °C for 30 min. After adding 176 μL of 10 mM acetate buffer solution (pH = 4.0), 4 μL of 1 mM BAA and 20 μL of 10 mM TMB, the above mixture solution was reacted for 3 min under visible light and followed by recording the A_{652} value.

2.8. Human serum sample detection

The drug-free human serum samples were derived from healthy individuals (n = 12) and prostate cancer patients (n = 18) at Fuzhou Second Hospital Affiliated to Xiamen University. Then, the samples were filtered with 0.45 μm filter for 3 times. Our study found that filtration had no effect on ACP activity (Fig. S1). All serum samples used in the experiment were diluted 50-fold with 10 mM acetate buffer solution (pH = 4.0). As described above, these samples were detected by using diluted human serum samples as ACP alternatives. The above experiments were carried out complying with the relevant laws and institutional guidelines and approved by the Ethics Committee of Fuzhou Second Hospital Affiliated to Xiamen University (20180016).

3. Results and discussion

3.1. Characterization of BAA

The synthesis route of BAA was exhibited in Fig. 1 via

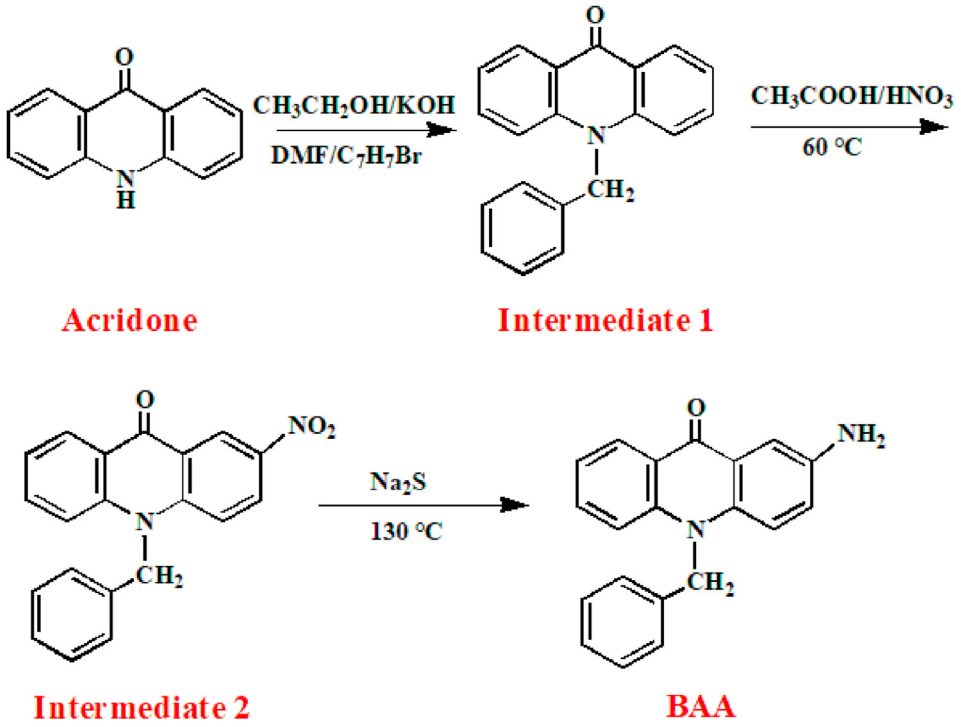

Fig. 1. The synthesis route of BAA.

substitution and reduction reactions. Firstly, the nitro and benzyl groups were modified on 2, 10-positions of acridone by substitution reaction, respectively. Then, utilizing the reducibility of Na_2S, the nitro was transformed to amino group, and the pure BAA was obtained by preparative HPLC (Fig. S2). To further confirm the structure of BAA, we utilized FT-IR, FAB-MS, ^1H NMR, and ^{13}C NMR spectroscopy for characterization (Fig. S3~S6). As expected, the benzyl and amino groups were successfully modified on acridone. In addition, in comparison with acridone and other intermediates, the color of BAA solid exhibited a clear change (Fig. S7) and its solution was transparent (Fig. S8), indicating that the introduction of amino group improved its water solubility. Above results demonstrated that BAA was synthesized successfully.

Next, we studied the optical properties of BAA. As shown in Fig. S9, acridone displayed obvious absorption peaks at 250 nm and 380 nm (Fig. S9A, curve a) and showed blue emission (Fig. S9B, curve a). Unlike acridone, the absorption (Fig. S9A, curve b) and emission (Fig. S9B, curve b) behavior of intermediate 1 presented slight red-shift ascribing to weak electron-donating effect of benzyl [30]. While the intermediate 2 presented significantly weak UV–vis absorption (Fig. S9A, curve c) and fluorescence emission (Fig. S9B, curve c), which attributed to the strong electron-withdrawing effect of nitro group [31]. In comparison with acridone and other intermediates, the UV–vis absorption peak of BAA showed a significant red shift (Fig. S9A, curve d) and its fluorescence emission changed from blue emission to green emission (Fig. S9B, curve d), which were similar to our previous report [28]. It is because amino group is an auxochrome group with strong electron-donating effect [32], enabling its optical behavior changed greatly. Furthermore, fluorescence of BAA showed a significant blue-shift under acidic conditions. And its green emission declined, but a new blue emission spectrum was observed (Fig. S10). Note that it was similar to related report that the amino group was prone to protonation under acidic conditions, causing changes in fluorescence emission [33]. Apparently, these experimental results further confirmed that BAA was synthesized as expected.

3.2. Visible-light-stimulated oxidase-like activity of BAA

For sake of evaluate the photocatalytic activity of BAA, we employed TMB, OPD and ABTS as chromogenic substrates, respectively. As shown in Fig. 2A ~ C, under visible light triggering, the BAA could oxidize TMB, OPD and ABTS in the absence of H_2O_2, resulting in blue products oxTMB (Fig. 2A, inset a), yellow products oxidized OPD (oxOPD) (Fig. 2B, inset a), and green products oxidized ABTS (oxABTS) (Fig. 2C, inset a), respectively. Accordingly, the absorption of oxTMB (Fig. 2A, curve a), oxOPD (Fig. 2B, curve a) and oxABTS (Fig. 2C, curve a) were measured. In contrast, without visible light irradiation, neither the absorption of oxTMB, oxOPD and oxABTS nor their solution color have changed, showing that the visible light was critical in reaction process and could regulate catalytic activity of BAA (Fig. 2A ~ C, inset and curve b). While without the BAA, the reaction solution showed almost colorless and no obvious absorption (Fig. 2A ~ C, inset and curve c). All the above results suggested that BAA endowed visible-light-stimulated oxidase-like activity. For exploring the photocatalytic mechanism of BAA, we selected TMB as chromogenic substrate. A series of scavengers were utilized to inhibit corresponding reactive species originating from the catalytic reaction such as hydroxyl radicals (•OH), singlet oxygen ($^1O_2$), H_2O_2, superoxide anions ($O_2^{\bullet-}$) and photo-generated holes (h^+) [34,35]. As illustrated in Fig. 2D, when the •OH scavenger IPA or TBA, H_2O_2 scavenger CAT, and $^1O_2$ inhibitor NaN_3 was added into the reaction system separately, the oxidation of TMB was affected negligibly, indicating that •OH, H_2O_2 and $^1O_2$ could not be generated in the catalytic process. However, an obviously declined absorption peak of oxTMB was observed by introducing of h^+ inhibitors such as EDTA, AO and KI, or nitrogen atmosphere (N_2), or $O_2^{\bullet-}$ inhibitor SOD, implying that h^+, dissolved oxygen (O_2), and $O_2^{\bullet-}$ were involved in the reaction process. It was like to some mimetic oxidase reported in the literature [21]. In

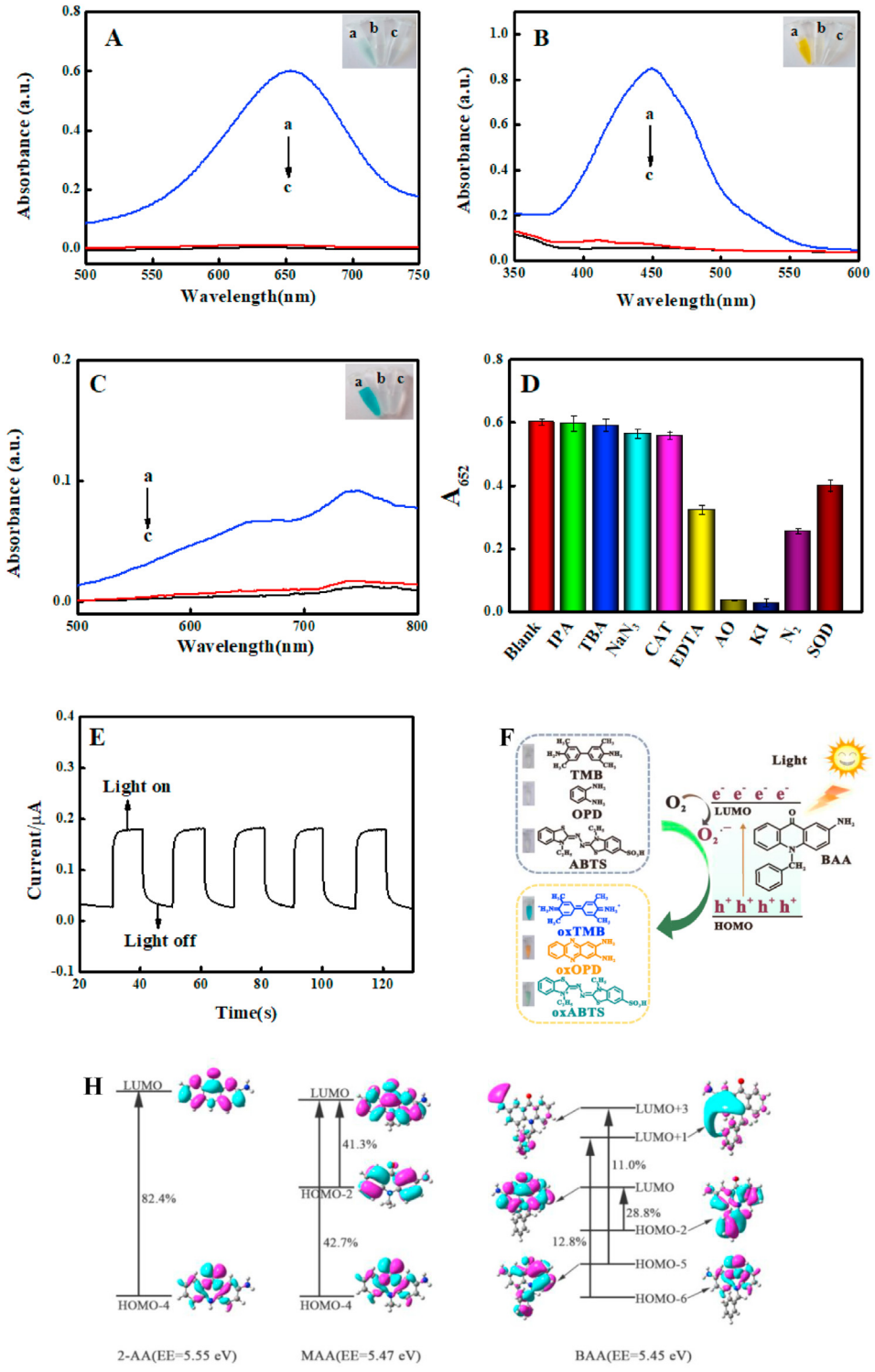

Fig. 2. The UV–vis absorption spectra of (A) TMB: (a) 10 μM BAA+500 μM TMB under visible light irradiation, (b) 10 μM BAA+500 μM TMB without visible light irradiation, and (c) 500 μM TMB under visible light irradiation. (B) OPD: (a) 10 μM BAA+500 μM OPD under visible light irradiation, (b) 10 μM BAA+500 μM OPD without visible light irradiation, and (c) 500 μM OPD under visible light irradiation. (C) ABTS: (a) 10 μM BAA+1 mM ABTS under visible light irradiation, (b) 10 μM BAA+1 mM ABTS without visible light irradiation, and (c) 1 mM ABTS under visible light irradiation. Inset: the corresponding optical photographs of each solution. (D) Effects of different scavengers on the visible-light-stimulated oxidase-like activity of BAA. (E) Photocurrent response of 10 μL 1 mM BAA modified on ITO electrode in 10 mM pH = 4.0 acetate buffer solutions under visible light illumination. (F) The catalytic mechanism of visible light-stimulated oxidase-like activity of BAA. (H) The electron excitation energy of 2-AA, MAA and BAA.

addition, we carries on the photoelectric chemistry experiment, the result was shown in Fig. 2E. A regulatable and stable rise/fall photocurrent signal was obtained with the irradiation light on and off cycle, which confirmed that the system was involved in the charge generation and transfer. In summary, the possible catalytic mechanism of BAA-mediated substrate oxidation was shown in

Fig. 2F. Under visible light triggering, the BAA could absorb photon energy, which made electrons (e^-) transition from the highest occupied molecular orbital (HOMO) to the lowest unoccupied molecular orbital (LUMO), and the photogenerated electrons reacted with dissolved O_2 to create $O_2^{\bullet-}$ for catalyzing oxidation TMB. Meanwhile, the photo-activated BAA also could yield h^+ to stay in HOMO that could be responsible for TMB oxidation, which was consistent with the previous report [28].

Next, we further investigated a series of steady-state kinetic parameters in catalytic reaction through changing TMB concentrations. Fig. S11 showed a representative Michaelis-Menten curve, the relevant kinetic parameters such as Michaelis-Menten constant K_m, maximum initial velocity V_{max}, catalytic constant K_{cat} and catalytic efficiency K_{cat}/K_m were calculated by the Lineweaver-Burk equation. From Table 1 can see, the K_{cat}/K_m value of BAA as oxidase mimic was measured to be 0.0609, which was higher than MAA and 2-aminoacridone (2-AA). It revealed that the BAA had high catalytic efficiency for TMB substrate, which was superior to our previous work [28]. To further illustrate the above phenomenon, we compared the electron excitation energy (EE) of BAA with MAA and 2-AA by quantum chemical calculation program Gaussin 09 [36]. Fig. 2H shows that the EE value of BAA was 5.45 eV, which was lower than MAA (5.47 eV) and 2-AA (5.55 eV). It suggested that the photo-activated BAA was the easiest to produce electrons for generating $O_2^{\bullet-}$. The results showed that photocatalytic performance of acridone derivatives were closely related to their functional groups.

3.3. Inhibitory effect of AA on the visible-light-stimulated oxidase-like activity of BAA

AA, also called vitamin C, is an excellent antioxidant and plays a vital role in the redox metabolism in vivo [37]. Some experiments were performed to investigate the inhibitory effect of AA on catalytic reaction system in this work. As shown in Fig. 3A, along with the increase of AA concentration the absorption of oxTMB decreased. As expected, it could clearly observed that the blue products gradually became colorless (inset in Fig. 3A). Correspondingly, a good linear relationship between ΔA_{652} and the AA concentrations was plotted in Fig. 3B (where ΔA_{652} is the difference of absorbance value at 652 nm without and with AA in the reaction solution). The linear equation was $\Delta A = 0.0168\ [AA]+0.0606$ ($r = 0.9991$) ranging from 1.0 to 30.0 μM and LOD was 0.86 μM. After that, we investigated the inhibitory mechanism of AA in the reaction system. As shown in Fig. 3C, after illumination, the produced oxTMB was reduced as the adding of AA, and the blue solution became colorless. While the illumination again, the solution returned to blue. To further explain the above phenomena, we also used fluorescein as a mimic enzyme possessing the same mechanism as BAA [21]. As expected, the absorbance of oxTMB also decreased with the introducing of AA, and accompanied by obvious color changes (Fig. S12). These results demonstrated that the oxTMB could be reduced by AA and the reaction system was controllable and regenerated by adjusting visible light. And its possible reaction mechanism was shown in Fig. S13, which was consistent with those reported in literature [38]. Besides, we also discovered that AA could react with $O_2^{\bullet-}$ to directly influence on the catalytic system. To understand this phenomenon, we conducted an electron spin resonance spectroscopy (ESR) experiment. As shown in Fig. 3D, a typical DMPO-$O_2^{\bullet-}$ peak was observed by using DMPO as spin trapping agent, which further manifested that BAA could catalyze O_2 to generate $O_2^{\bullet-}$ radicals under visible light irradiation. While the ESR signal was decreased obviously after adding the AA, which confirmed that $O_2^{\bullet-}$ could be inhibited by AA. As a result, we could suppose that AA was able to reduce oxTMB and react with $O_2^{\bullet-}$, resulting in decreasing the production of oxTMB, thus inhibiting the reaction system.

3.4. ACP detection and inhibitor screening

ACP, as an essential and universal hydrolase, can catalyze the hydrolysis of phosphomonoester to inorganic phosphate under acidic conditions [39]. In the work, we selected AAP as ACP substrate, which could be catalyzed by ACP to generate phosphate and AA. As exhibited above, upon the introduction of AA, the photocatalytic activity of BAA could be hampered. That is, the ACP-mediated enzymatic reaction would directly interfered TMB oxidation. As shown in Fig. 4, the BAA could catalyze oxidation of TMB to generate blue oxTMB (Fig. 4A, curve a). And neither AAP (Fig. 4A, curve b) nor ACP (Fig. 4A, curve c) influenced the reaction system. However, in presence of both AAP and ACP, the catalytic system could produce AA, the catalytic activity of BAA inhibited (Fig. 4A, curve d). Moreover, in the absence of BAA, the mixed solution of AAP and ACP no effected on the TMB oxidation (Fig. 4A, curve e). At the same time, the above reaction process could be readout directly with the naked eye (inset in Fig. 4A). All the phenomena verified that a colorimetric sensor can be constructed for ACP detection based on photocatalytic activity of BAA (Scheme 1). Fig. 4B exhibited that the absorption of oxTMB was remarkably decay as the ACP concentrations increased, and its the solution color faded gradually. Meanwhile, the ΔA_{652} was proportional to ACP concentrations in the range from 0.05 to 2.5 U/L (Fig. 4C) (where ΔA_{652} is the difference of absorbance value at 652 nm before and after adding ACP in the reaction solution). The linear equation was $\Delta A = 0.1513\ [ACP]+0.0359$ ($r = 0.9994$). The relative standard deviation (RSD) was 2.46% for detecting of 2 U/L ACP ($n = 5$), proving that this method has good repeatability. And the LOD was 0.0415 U/L ($S/N = 3$). Compared to other works (Table S1), our proposed method for ACP activity detection exhibited a satisfying result [4,40–52]. Although some works were superior to our method in some ways, they still suffered from some defects: (1) the most electrochemical analysis had some inevitable problems, such as complex sample interference and poor reproducibility [40–42]. (2) some of them depended on a large amount of H_2O_2, leading to a harsh reaction condition [44,50]. (3) some detection systems required the involvement of nanozymes with high biological toxicity [45,52]. (4) some colorimetric reactions lacked controllability [51]. According to the above comparison, our proposed method showed mild reaction conditions and good controllable. To assess the selectivity of the sensing system, we utilized different enzymes, such as urease, pyrophosphohydrolase, lysozyme, α-glucosidase, proteinase K, CAT, alkaline phosphatase and

Table 1
Comparison of the K_m, V_{max}, K_{cat} and K_{cat}/K_m of BAA and other acridone derivatives.

Catalyst	Substrate	K_m [mM]	V_{max} [10^{-8} M S^{-1}]	K_{cat} [10^{-2} S^{-1}]	K_{cat}/K_m [$mM^{-1}\cdot S^{-1}$]	Ref.
2-AA	TMB	0.2119 ± 0.006	4.278 ± 0.136	0.4278	0.0202	[28]
MAA	TMB	0.141 ± 0.008	4.998 ± 0.150	0.4998	0.0354	[28]
BAA	TMB	0.294 ± 0.005	17.909 ± 0.108	1.7909	0.0609	This work

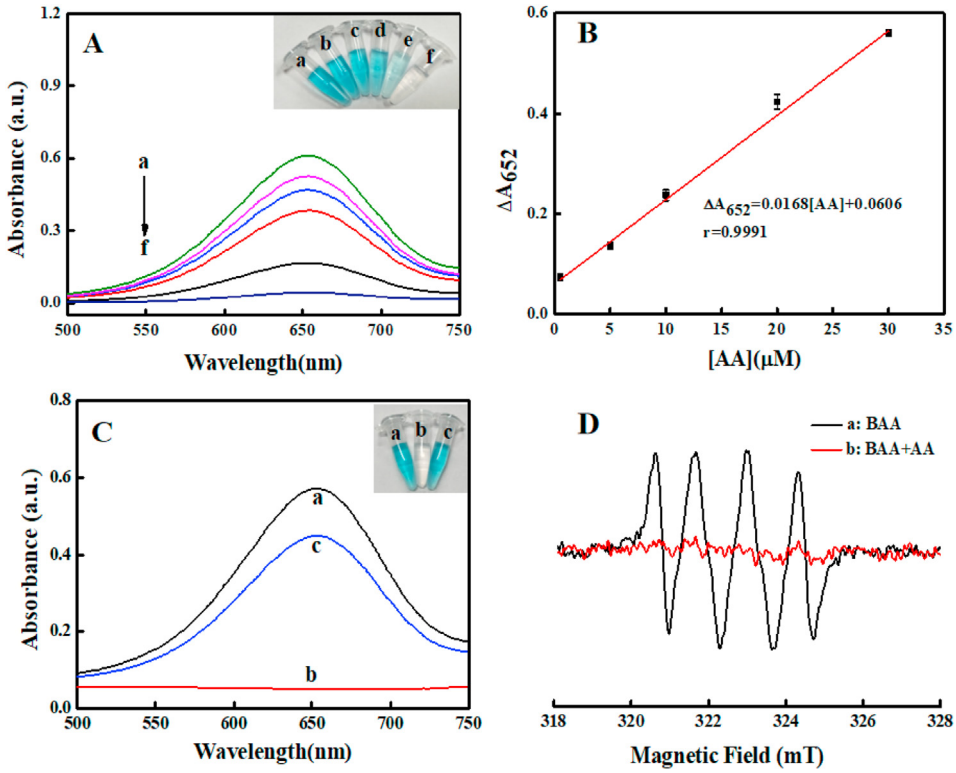

Fig. 3. (A) UV−vis spectra of oxTMB in the presence of different AA concentrations. From a to f: 0, 1.0, 5.0, 10.0, 20.0, 30.0 μM. (B) The linear relationship between ΔA_{652} and the AA concentrations in the range from 1.0 to 30.0 μM. (C) The UV−vis spectra of (a) 10 μM BAA and 500 μM TMB reacted for 3 min under visible light illumination, (b) 10 μM BAA and 500 μM TMB reacted for 3 min under visible light illumination, then added 32.5 μM AA, and (c) 10 μM BAA and 500 μM TMB reacted for 3 min under visible light illumination, then added 32.5 μM AA, and finally irradiated by visible light for 3 min again. Inset: the corresponding optical photographs of each solution. (D) The ESR spectra of (a) BAA and (b) BAA + AA with spin trap DMPO after visible light irradiation for 5 min.

horseradish peroxidase, as ACP alternatives under the same condition. Fig. 4D exhibited that the absorption signal of oxTMB was changed dramatically as the ACP added and the other enzymes showed negligible variations. Furthermore, some proteins, common metal ions and small molecules (except GSH, L-cysteine and AA) also did not produce an evident signal change (Fig. S14). Although GSH and L-cysteine had obvious interference to the sensing system (Fig. S14 (18−19)), the interference of thiol species could be eliminated by using NEM as the masking agent [4,54]. As shown in Fig. S14 (20−21), after incubation of GSH or L-cysteine with NEM, the UV absorption of oxTMB gave a negligible signal change. For AA, it has an effect on the detection system at high concentration. However, considering that its physiological level in plasma is about 50 μM [55], and its instability in vitro plasma [56], and the samples were diluted 50 times in the actual sample testing, we investigated the effect of 1 μM AA on the sensing system. The result showed that the low concentration of AA has little effect on the detection system (Fig. S14 (22)). These results demonstrated that the proposed colorimetric biosensor showed a good selectivity for ACP detection.

To verify the feasibility of this sensing system for the screening of potential ACP inhibitors, we selected NaF as an ACP inhibitor. It is generally known that the NaF could affect the hydrolysis of AAP by ACP [47]. As shown in Fig. S15, with the adding of NaF into the reaction solution, the generation of AA could be prevented, the A_{652} value of oxTMB would be increased. And the half-maximal inhibition value (IC_{50}) was calculated to be 35.6 μM. The result apparently manifested that the colorimetric sensing system could be utilized for screening the corresponding ACP inhibitor.

3.5. ACP activity assay in human serum sample

To validate the feasibility of the proposed colorimetric system in practical application, we investigated ACP activity in human serum samples deriving from healthy individuals (n = 12) and prostate cancer patients (n = 18). Fig. 5 showed that the average ACP expression level in healthy individual and prostate cancer patient (mean ± SD) were 5.17 ± 0.234 U/L and 9.32 ± 0.541 U/L, respectively. And the experiment had statistical significance ($p < 0.0001$). Obviously, it was the same as previous reports that the ACP concentration from prostate cancer patient was higher than that from healthy control group [57,58]. Also, the data agreed fairly well with results obtained using the standard ACP assay kit (Table S2). Therefore, the sensing system is of great potential for clinical application.

4. Conclusions

In short, we synthesized an acridone derivative with benzyl and amino groups, called BAA. We found that the synthesized BAA exhibited an intrinsic photocatalytic activity, which catalyzed oxidation of different substrates without destructive H_2O_2 under visible light illumination. The catalytic mechanism showed that $O_2^{\bullet-}$ and h^+ were the main reactive species for oxidizing TMB. The experimental result of Michaelis-Menten kinetics indicated that the BAA had a higher catalytic efficiency for TMB substrate than our previous work. And we found that the functional groups could regulate the photocatalytic performance of BAA. On the basis of catalytic activity of BAA, we developed a cost-effective, green, and

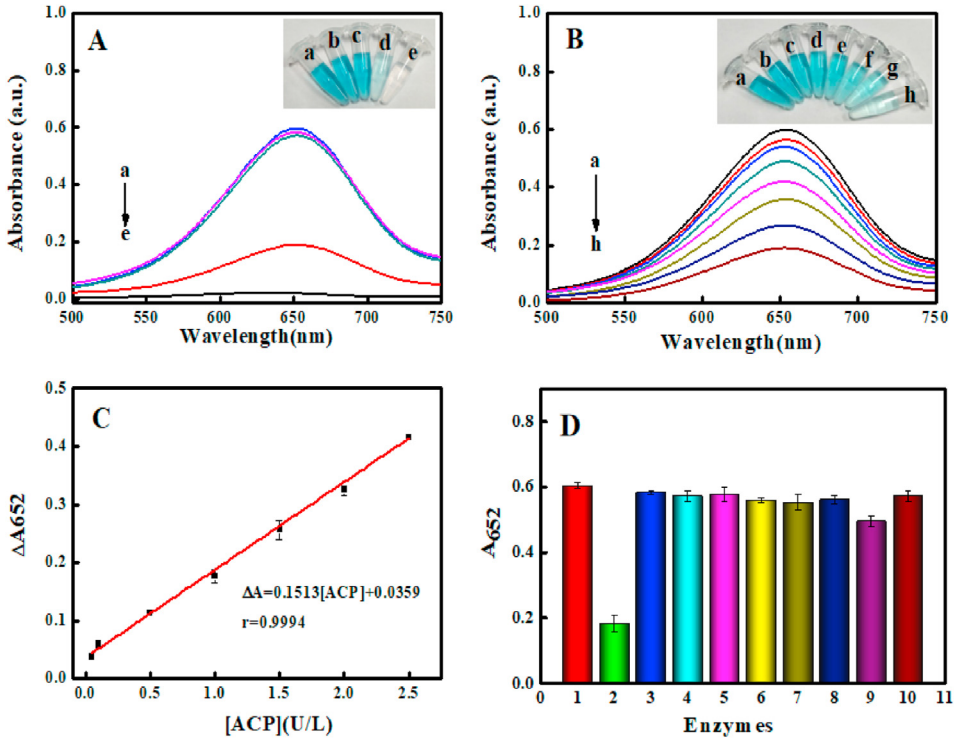

Fig. 4. (A) UV–vis spectra of (a) 10 μM BAA+500 μM TMB, (b) 10 μM BAA+500 μM TMB+1 mM AAP, (c) 10 μM BAA+500 μM TMB+2.5 U/L ACP, (d) 10 μM BAA+500 μM TMB+1 mM AAP+2.5 U/L ACP, (e) 500 μM TMB+1 mM AAP+2.5 U/L ACP. Inset: the corresponding optical photographs of each reaction solution. (B) Effects of different ACP concentrations on the visible-light-induced oxidase-like activity of BAA. From a to h: 0, 0.05, 0.1, 0.5, 1.0, 1.5, 2.0, 2.5 U/L. (C) The linear relationship between ΔA_{652} and the ACP concentrations in the range from 0.05 to 2.5 U/L. (D) Selectivity of the colorimetric sensing for ACP detection. From 1 to 10: blank, ACP, urease, pyrophosphohydrolase, lysozyme, α-glucosidase, proteinase K, CAT, alkaline phosphatase, and horseradish peroxidase. The concentration of ACP was 2.5 U/L and the others were 50 U/L.

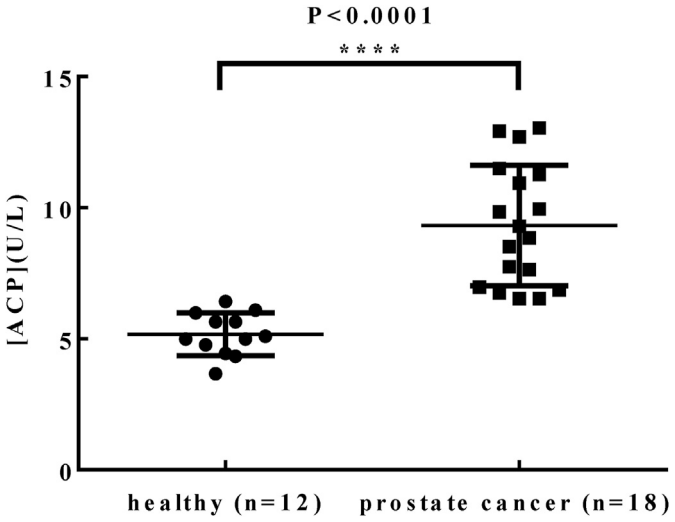

Fig. 5. The ACP concentrations in serum samples from heathy controls (n = 12) and prostate cancer patients (n = 18). P < 0.0001, P-value was calculated by unpaired two-tailed *t*-test.

facile colorimetric sensor for monitoring ACP activity in serum samples. This study not only broadened the application of acridone derivatives, but also provided a research basis for future biosensors and biomedical fields. Considering the modification flexibility of the structure of acridone derivatives, we will be introduce appropriate groups to further improve its photocatalytic activity. Besides, we also found that BAA possessed high electrochemical activity, stable photochemistry and good non-linear optical properties, which was a promising multi-functional probe and was expected to be used in the construction of multi-mode sensing platform. Meanwhile, we believe that it was a potential and feasible to construct a new biosensor platform for real-time detection of multiple biomarkers based on acridone derivatives, aptamer technology, and DNA self-assembly technology.

CRediT authorship contribution statement

Tao Zhang: Conceptualization, Writing – original draft, Practical sample, detection. **Wenhui He:** Validation, Writing – original draft. **Xiaodan Song:** Methodology, Visualization. **Dongzhi Wu:** Methodology, Investigation. **Yaokun Xia:** Visualization, Formal analysis. **Yan Liu:** Visualization, Formal analysis. **Linzhao Wu:** Data curation. **Weiming Sun:** Formal analysis, Writing – review & editing. **Fengfei Lin:** Sample collection, Writing – review & editing, Project administration. **Jinghua Chen:** Resources, Writing – review & editing, Funding acquisition, Supervision.

Declaration of competing interest

The authors declare that they have no known competing financial interests or personal relationships that could have appeared to influence the work reported in this paper.

Acknowledgements

The authors gratefully acknowledge the financial support of the National Natural Science Foundation of China (Nos. 21874019), the Natural Science Foundation of Fujian Province (Nos. 2016J01594, 2017J07001, and 2019J01546), Young Top-notch Talent Project of

Colleges and Universities of Fujian Province (3002360301), the Project of innovation platform for Fuzhou Health and Family Planning Commission (Nos. 2017-S-wp1).

Appendix A. Supplementary data

Supplementary data to this article can be found online at https://doi.org/10.1016/j.aca.2021.338357.

References

[1] Y.K. Xia, T.T. Chen, G.Y. Chen, Y.P. Weng, L.P. Zeng, Y.J. Liao, W.Q. Chen, J.M. Lan, J. Zhang, J.H. Chen, A nature-inspired colorimetric and fluorescent dual-modal biosensor for exosomes detection, Talanta 214 (2020) 120851–120893, https://doi.org/10.1016/j.talanta.2020.120851.

[2] W. Hong, S. Lee, Y. Cho, Dual-responsive immunosensor that combines colorimetric recognition and electrochemical response for ultrasensitive detection of cancer biomarkers, Biosens. Bioelectron. 86 (2016) 920–926, https://doi.org/10.1016/j.bios.2016.07.014.

[3] X.Q. Wang, Z.W. Luo, Q.Y. Xie, Z.J. Huang, M.F. Wu, Y.X. Duan, Toehold-mediated strand displacement reaction formation of three-way junction DNA structure combined with nicking enzyme signal amplification for highly sensitive colorimetric detection of Salmonella Typhimurium, Anal. Chim. Acta 1139 (2020) 138–145, https://doi.org/10.1016/j.aca.2020.09.023.

[4] J. Li, Y.Y. W, Z.R. Xu, Visual detection of acid phosphatase based on hollow mesoporous manganese dioxide nanospheres, Anal. Chim. Acta 1138 (2020) 1–8, https://doi.org/10.1016/j.aca.2020.09.010.

[5] G.J. Cao, X. Jiang, H. Zhang, T.R. Croley, J.J. Yin, Mimicking horseradish peroxidase and oxidase using ruthenium nanomaterials, RSC Adv. 7 (2017) 52210–52217, https://doi.org/10.1039/c7ra10370k.

[6] I. Nath, J. Chakraborty, F. Verpoort, Metal organic frameworks mimicking natural enzymes: a structural and functional analogy, Chem. Soc. Rev. 45 (2016) 4127–4170, https://doi.org/10.1039/C6CS00047A.

[7] F. Tian, J. Zhou, B. Jiao, Y. He, A nanozyme-based cascade colorimetric aptasensor for amplified detection of ochratoxin A, Nanoscale 11 (2019) 9547–9555, https://doi.org/10.1039/C9NR02872B.

[8] Y. Xia, M. Liu, L. Wang, A. Yan, W. He, M. Chen, J. Lan, J. Xu, L. Guan, J. Chen, A visible and colorimetric aptasensor based on DNA-capped single-walled carbon nanotubes for detection of exosomes, Biosens. Bioelectron. 92 (2017) 8–15, https://doi.org/10.1016/j.bios.2017.01.063.

[9] W. Zhang, S. Hu, J.J. Yin, W. He, W. Lu, M. Ma, N. Gu, Y. Zhang, Prussian blue nanoparticles as multienzyme mimetics and reactive oxygen species scavengers, J. Am. Chem. Soc. 138 (2016) 5860–5865, https://doi.org/10.1021/jacs.5b12070.

[10] H. Cheng, Y. Liu, Y. Hu, Y. Ding, S. Lin, W. Cao, Q. Wang, J. Wu, F. Muhammad, X. Zhao, D. Zhao, Z. Li, H. Xing, H. Wei, Monitoring of heparin activity in live rats using metal-organic framework nanosheets as peroxidase mimics, Anal. Chem. 89 (2017) 11552–11559, https://doi.org/10.1021/acs.analchem.7b02895.

[11] L. Liu, Y. Shi, Y. Yang, M. Li, Y. Long, Y. Huang, H. Zheng, Fluorescein as an artificial enzyme to mimic peroxidase, Chem. Commun. 52 (2016) 13912–13915, https://doi.org/10.1039/C6CC07896F.

[12] S. Cai, C. Qi, Y. Li, Q. Han, R. Yang, C. Wang, PtCo bimetallic nanoparticles with high oxidase-like catalytic activity and their applications for magnetic-enhanced colorimetric biosensing, J. Mater. Chem. B 4 (2016) 1869–1877, https://doi.org/10.1039/C5TB02052B.

[13] L.Y. Jin, Y.M. Dong, X.M. Wu, G.X. Cao, G.L. Wang, Versatile and amplified biosensing through enzymatic cascade reaction by coupling alkaline phosphatase in situ generation of photoresponsive nanozyme, Anal. Chem. 87 (2015) 10429–10436, https://doi.org/10.1021/acs.analchem.5b02728.

[14] J. Du, J. Wang, W. Huang, Y. Deng, Y. He, Visible light-cctivatable oxidase mimic of 9-mesityl-10-methylacridinium ion for colorimetric detection of biothiols and logic operations, Anal. Chem. 90 (2018) 9959–9965, https://doi.org/10.1021/acs.analchem.8b02197.

[15] Y. Liu, M. Zhou, W. Cao, X. Wang, Q. Wang, S. Li, H. Wei, Light-responsive metal-organic framework as an oxidase mimic for cellular glutathione detection, Anal. Chem. 91 (2019) 8170–8175, https://doi.org/10.1021/acs.analchem.9b00512.

[16] J. Zhang, X. Lu, D. Tang, S. Wu, X. Hou, J. Liu, P. Wu, Phosphorescent carbon dots for highly efficient oxygen photosensitization and as photo-oxidative nanozymes, ACS Appl. Mater. Interfaces 10 (2018) 40808–40814, https://doi.org/10.1021/acsami.8b15318.

[17] G.L. Wang, L.Y. Jin, Y.M. Dong, X.M. Wu, Z.J. Li, Intrinsic enzyme mimicking activity of gold nanoclusters upon visible light triggering and its application for colorimetric trypsin detection, Biosens. Bioelectron. 64 (2015) 523–529, https://doi.org/10.1016/j.bios.2014.09.071.

[18] G.X. Cao, X.M. Wu, Y.M. Dong, Z.J. Li, G.L. Wang, In situ enzymatically generated photoswitchable oxidase mimetics and their application for colorimetric detection of glucose oxidase, Molecules 21 (2016), e902, https://doi.org/10.3390/molecules21070902.

[19] G.L. Wang, X.F. Xu, L. Qiu, Y.M. Dong, Z.J. Li, C. Zhang, Dual responsive enzyme mimicking activity of AgX (X=Cl, Br, I) nanoparticles and its application for cancer cell detection, ACS Appl. Mater. Interfaces 6 (2014) 6434–6442, https://doi.org/10.1021/am501830v.

[20] F. Peng, M.I. Setyawati, J.K. Tee, X. Ding, J. Wang, M.E. Nga, H.K. Ho, D.T. Leong, Nanoparticles promote in vivo breast cancer cell intravasation and extravasation by inducing endothelial leakiness, Nat. Nanotechnol. 14 (2019) 279–286, https://doi.org/10.1038/s41565-018-0356-z.

[21] L. Liu, C. Sun, J. Yang, Y. Shi, Y. Long, H. Zheng, Fluorescein as a visible-light-induced oxidase mimic for signalamplified colorimetric assay of carboxylesterase by enzymatic cascade reaction, Chem. Eur J. 24 (2018) 6148–6154, https://doi.org/10.1002/chem.201705980.

[22] X. Zhang, C. Huang, S. Xu, J. Chen, Y. Zeng, P. Wu, X. Hou, Photocatalytic oxidation of TMB with the double stranded DNA-SYBR Green I complex for label-free and universal colorimetric bioassay, Chem. Commun. 51 (2015) 14465–14468, https://doi.org/10.1039/c5cc06105a.

[23] J. Chen, J. Zhang, L. Huang, X. Lin, G. Chen, Hybridization biosensor using 2-nitroacridone as electrochemical indicator for detection of short DNA species of Chronic Myelogenous Leukemia, Biosens. Bioelectron. 24 (2008) 349–355, https://doi.org/10.1016/j.bios.2008.04.008.

[24] J. Chen, X. Zhang, S. Cai, D. Wu, J. Lin, C. Li, J. Zhang, Label-free electrochemical biosensor using home-made 10-methyl-3-nitro-acridone as indicator for picomolar detection of nuclear factor kappa B, Biosens, Bioelectron 53 (2014) 12–17, https://doi.org/10.1016/j.bios.2013.09.038.

[25] C. Huang, S.J. Yan, X.H. Zeng, B. Sun, M.B. Lan, J. Lin, Synthesis and evaluation of the antitumor activity of polyhalo acridone derivatives, RSC Adv. 5 (2015) 17444–17450, https://doi.org/10.1039/C4RA12354A.

[26] C. Li, Z. Liu, S. Cai, F. Wen, D. Wu, Y. Liu, F. Wu, J. Lan, Z. Han, J. Chen, An electrochemical microRNA biosensor based on protein p19 combining an acridone derivate as indicator and DNA concatamers for signal amplification, Electrochem. Commun. 60 (2015) 185–189, https://doi.org/10.1016/j.elecom.2015.09.012.

[27] Y. Xia, L. Wang, J. Li, X. Chen, J. Lan, A. Yan, Y. Lei, S. Yang, H. Yang, J. Chen, A ratiometric fluorescent bioprobe based on carbon dots and acridone derivate for signal amplification detection exosomal microRNA, Anal. Chem. 90 (2018) 8969–8976, https://doi.org/10.1021/acs.analchem.8b01143.

[28] Y.K. Xia, W.H. He, J. Li, L.P. Zeng, T.T. Chen, Y.J. Liao, W.M. Sun, J.M. Lan, S.M. Zhuo, J. Zhang, H.H. Yang, J.H. Chen, Acridone derivate simultaneously featuring multiple functions and its applications, Anal. Chem. 91 (2019) 8406–8414, https://doi.org/10.1021/acs.analchem.9b01289.

[29] Y.K. Xia, T.T. Chen, L. Zhang, X.L. Zhang, W.H. Shi, G.Y. Chen, W.Q. Chen, J.M. Lan, C.Y. Li, W.M. Sun, J.H. Chen, Colorimetric detection of exosomal microRNA through switching the visible-light-induced oxidase mimic activity of acridone derivate, Biosens. Bioelectron. 173 (2021) 112834–112844, https://doi.org/10.1016/j.bios.2020.112834.

[30] X.Y. Chen, X.J. Peng, A.J. Cui, B.S. Wang, L. Wang, R. Zhang, Photostabilities of novel heptamethine 3H-indolenine cyanine dyes with different N-substituents, J. Photochem. Photobiol., A 181 (2006) 79–85, https://doi.org/10.1016/j.jphotochem.2005.11.004.

[31] Z. Thiel, P. Rivera-Fuentes, Single-molecule imaging of active mitochondrial nitroreductases using a photo-crosslinking fluorescent sensor, Angew. Chem. Int. Ed. 58 (2019) 11474–11478, https://doi.org/10.1002/anie.201904700.

[32] W. Zeng, G. Chen, Y. Zhang, K. Wu, Z. Liang, Studies on the UV spectrum of poly(γ-glutamic acid) based on development of a simple quantitative method, Int. J. Biol. Macromol. 51 (2012) 83–90, https://doi.org/10.1016/j.ijbiomac.2012.04.005.

[33] X.Y. Xu, B. Yan, An efficient and sensitive fluorescent pH sensor based on amino functional metal-organic frameworks in aqueous environment, Dalton Trans. 45 (2016) 7078–7084, https://doi.org/10.1039/C6DT00361C.

[34] H.H. Deng, X.L. Lin, Y.H. Liu, K.L. Li, Q.Q. Zhuang, H.P. Peng, A.L. Liu, X.H. Xia, W. Chen, Chitosan-stabilized platinum nanoparticles as effective oxidase mimics for colorimetric detection of acid phosphatase, Nanoscale 9 (2017) 10292–10300, https://doi.org/10.1039/c7nr03399k.

[35] N. Singh, M.A. Savanur, S. Srivastava, P. D'Silva, G. Mugesh, A redox modulatory Mn_3O_4 nanozyme with multi-enzyme activity provides efficient cytoprotection to human cells in a Parkinson's disease model, Angew. Chem. Int. Ed. 56 (2017) 14267–14271, https://doi.org/10.1002/anie.201708573.

[36] M.J. Frisch, G.W. Trucks, H.B. Schlegel, et al., Gaussian 09, Revision C. 01, Gaussian Inc., Wallingford, CT, 2010, 2009.

[37] X. Zhu, T. Zhao, Z. Nie, Y. Liu, S. Yao, Non-redox modulated fluorescence strategy for sensitive and selective ascorbic acid detection with highly photoluminescent nitrogen-doped carbon nanoparticles via solid-state synthesis, Anal. Chem. 87 (2015) 8524–8530, https://doi.org/10.1021/acs.analchem.5b02167.

[38] Y. Ma, M. Zhao, B. Cai, W. Wang, Z. Ye, J. Huang, 3D graphene network@WO3 nanowire composites: a multifunctional colorimetric and electrochemical biosensing platform, Chem. Commun. 50 (2014) 11135–11138, https://doi.org/10.1039/c4cc04507f.

[39] H. Bull, P.G. Murray, D. Thomas, A.M. Fraser, P.N. Nelson, Acid phosphatases, Mol. Pathol. 55 (2002) 65–71, https://doi.org/10.1136/mp.55.2.65.

[40] X.Y. Gan, F. Qiu, B.Y. Jiang, R. Yuan, Y. Xiang, Convenient and highly sensitive electrochemical biosensor for monitoring acid phosphatase activity,, Sensor. Actuator. B Chem. 332 (2021) 129483–129512, https://doi.org/10.1016/j.snb.2021.129483.

[41] Q. Bi, F. Qiu, R. Yuan, Y. Xiang, In situ formation of G-quadruplex/hemin nanowires for sensitive and label-free electrochemical sensing of acid

phosphatase, Sensor. Actuator. B Chem. 330 (2020) 127272–129301, https://doi.org/10.1016/j.snb.2020.129272.
[42] M.J. Huang, J.Y. Tian, C.H. Zhou, P. Bai, J.S. Lu, Photoelectrochemical determination for acid phosphatase activity based on an electron inhibition strategy, Sensor. Actuator. B Chem. 307 (2020) 127654–127661, https://doi.org/10.1016/j.snb.2020.127654.
[43] X. Yan, C. Xia, B. Chen, Y.F. Li, P.F. Gao, C.Z. Huang, Enzyme activity triggered blocking of plasmon resonance energy transfer for highly selective detection of acid phosphatase, Anal. Chem. 92 (2020) 2130–2135, https://doi.org/10.1021/acs.analchem.9b04685.
[44] S. Li, X. Hu, Q. Chen, X. Zhang, H. Chai, Y. Huang, Introducing bifunctional metal-organic frameworks to the construction of a novel ratiometric fluorescence sensor for screening acid phosphatase activity, Biosens. Bioelectron. 137 (2019) 133–139, https://doi.org/10.1016/j.bios.2019.05.010.
[45] J. Wang, Y. Yan, X. Yan, T. Hu, X. Tang, X. Su, Label-free fluorescent assay for high sensitivity and selectivity detection of acid phosphatase and inhibitor screening, Sensor. Actuator. B Chem. 234 (2016) 470–477, https://doi.org/10.1016/j.snb.2016.05.024.
[46] Y. Chen, Z. Wang, X. Hao, F. Li, Y. Zheng, J. Zhang, X. Lin, S. Weng, Selective and sensitive fluorescent monitoring of acid phosphatase (ACP) activity under neutral conditions through the ACP enzymatic catalysis of dopamine as a new substrate to polydopamine, Sensor. Actuator. B Chem. 297 (2019) 126784–126812, https://doi.org/10.1016/j.snb.2019.126784.
[47] Z.M. Zhu, X.Y. Lin, L.N. Wu, C.F. Zhao, Y.J. Zheng, A.L. Liu, L.Q. Lin, X.H. Lin, "Switch-On" fluorescent nanosensor based on nitrogen-doped carbon dots-MnO_2 nanocomposites for probing the activity of acid phosphatase, Sensor. Actuator. B Chem. 274 (2018) 609–615, https://doi.org/10.1016/j.snb.2018.08.011.
[48] Z. Qian, L. Chai, Q. Zhou, Y. Huang, C. Tang, J. Chen, H. Feng, Reversible fluorescent nanoswitch based on carbon quantum dots nanoassembly for realtime acid phosphatase activity monitoring, Anal. Chem. 87 (14) (2015) 7332–7339, https://doi.org/10.1021/acs.analchem.5b01488.
[49] Y. Xu, B. Li, L. Xiao, J. Ouyang, S. Sun, Y. Pang, A colorimetric and near-infrared fluorescent probe with high sensitivity and selectivity for acid phosphatase and inhibitor screening, Chem. Commun. 50 (2014) 8677–8680, https://doi.org/10.1039/C3CC49254K.
[50] S.S. Zheng, H.Z. Gu, D.Y. Yin, J.L. Zhang, W. Li, Y. Fu, Biogenic synthesis of AuPd nanocluster as a peroxidase mimic and its application for colorimetric assay of acid phosphatase, Colloids and Surfaces A Physicochemical and Engineering Aspects 589 (2020) 124444–124472, https://doi.org/10.1016/j.colsurfa.2020.124444.
[51] L. Jin, Y. Sun, L. Shi, C. Li, Y. Shen, PdPt bimetallic nanowires with efficient oxidase mimic activity for the colorimetric detection of acid phosphatase in acidic media, J. Mater. Chem. B 7 (2019) 4561–4567, https://doi.org/10.1039/C9TB00730J.
[52] Z. Lin, X.M. Zhang, S.J. Liu, L.L. Zheng, Y.M. Bu, H.H. Deng, R.T. Chen, H.P. Peng, X.H. Lin, W. Chen, Colorimetric acid phosphatase sensor based on MoO_3 nanozyme, Anal. Chim. Acta 1105 (2020) 162–168, https://doi.org/10.1016/j.aca.2020.01.035.
[54] T. Xiao, J. Sun, J.H. Zhao, S. Wang, G.R. Liu, X.R. Yang, FRET effect between fluorescent polydopamine nanoparticles and MnO_2 nanosheets and its application for sensitive sensing of alkaline phosphatase, ACS Appl. Mater. Interfaces 10 (7) (2018) 6560–6569, https://doi.org/10.1021/acsami.7b18816.
[55] S.J. Padayatty, M. Levine, Vitamin C: the known and the unknown and Goldilocks, Oral Dis. 22 (2016) 463–493, https://doi.org/10.1111/odi.12446.
[56] J. Lykkesfeldt, On the effect of vitamin C intake on human health: how to (mis) interprete the clinical evidence, Redox Biology 34 (2020) 101532–101571, https://doi.org/10.1016/j.redox.2020.101532.
[57] A.G. Foti, J.F. Cooper, H. Herschman, R.R. Malvaez, Detection of prostatic cancer by solid-phase radioimmunoassay of serum prostatic acid phosphatase, N. Engl. J. Med. 297 (1977) 1357–1361, https://doi.org/10.1056/NEJM197712222972501.
[58] H.Y. Kong, J. Byun, Emerging roles of human prostatic acid phosphatase, Biomol. Ther. 21 (2013) 10–20, https://doi.org/10.4062/biomolther.2012.095.